https://doi.org/10.5194/acp-2021-391
Preprint. Discussion started: 7 June 2021

Atmospheric Chemistry and Physics Discussions

Environmental Effects on Aerosol-Cloud Interaction in non-precipitating MBL Clouds over the Eastern North Atlantic

Xiaojian Zheng[1], Baike Xi[1], Xiquan Dong[1] and Peng Wu[2]

[1]Department of Hydrology and Atmospheric Sciences, University of Arizona, Tucson, AZ, USA
[2]Pacific Northwest National Laboratory, Richland, WA, USA

Correspondence: Baike Xi (baikex@arizona.edu)

Abstract. Over the eastern north Atlantic (ENA) ocean, a total of 20 non-precipitating single-layer marine boundary layer (MBL) stratus and stratocumulus cloud cases are selected in order to investigate the impacts of the environmental variables on the aerosol-cloud interaction ($\mathrm{ACI_r}$) using the ground-based measurements from the Department of Energy Atmospheric Radiation Measurement (ARM) facility at the ENA site during the period 2016 – 2018. The $\mathrm{ACI_r}$ represents the relative change of cloud-droplet effective radius r_e with respect to the relative change of cloud condensation nuclei (CCN) number concentration at 0.2% supersaturation ($N_{CCN,0.2\%}$) in the water vapor stratified environment. The $\mathrm{ACI_r}$ values vary from -0.004 to 0.207 with increasing precipitable water vapor (PWV) conditions, indicating that r_e is more sensitive to the CCN loading under sufficient water vapor supply, owing to the combined effect of enhanced condensational growth and coalescence processes associated with higher N_c and PWV. The environmental effects on $\mathrm{ACI_r}$ are examined by stratifying the data into different lower tropospheric stability (LTS) and vertical component of turbulence kinetic energy ($\mathrm{TKE_w}$) regimes. The higher LTS normally associates with a more adiabatic cloud layer and a lower boundary layer and thus results in higher CCN to cloud droplet conversion and $\mathrm{ACI_r}$. The $\mathrm{ACI_r}$ values under a range of PWV double from low $\mathrm{TKE_w}$ to high $\mathrm{TKE_w}$ regime, indicating a strong impact of turbulence on the $\mathrm{ACI_r}$. The stronger boundary layer turbulence represented by higher $\mathrm{TKE_w}$ strengthens the connection and interaction between cloud microphysical properties and the underneath CCN and moisture sources. With sufficient water vapor and low CCN loading, the active coalescence process broadens the cloud droplet size distribution spectra, and consequently results in an enlargement of r_e. The enhanced N_c conversion and condensational growth induced by more intrusions of CCN effectively decrease r_e, which jointly presents as the increased $\mathrm{ACI_r}$. The $\mathrm{TKE_w}$ median value of 0.08 $\mathrm{m^2 s^{-2}}$ suggests a feasible way in distinguishing the turbulence-enhanced aerosol-cloud interaction in non-precipitating MBL clouds.

https://doi.org/10.5194/acp-2021-391
Preprint. Discussion started: 7 June 2021

Atmospheric Chemistry and Physics Discussions

1. Introduction

Clouds are one of the most important parts of the Earth's climate system. They can impact the global climate by modulating the radiative balance in the atmosphere. Moreover, the radiative effects of cloud adjustments due to aerosols remain as one of the largest uncertainties in climate modeling (IPCC, 2013). Over the oceanic area, the lower troposphere is dominated by marine boundary layer (MBL) clouds. MBL clouds can persistently reflect the solar radiation by their long-lasting nature maintained by cloud-top radiative cooling, and therefore act as a major modulator of Earth radiative budget (Seinfeld et al., 2016). The climatic importance of the MBL cloud radiative properties is primarily induced by the cloud microphysical properties, namely the cloud-droplet number concentration (N_C) and effective radius (r_e), has been intensively investigated by many researchers (Rosenfeld, 2007; Wood et al., 2015; Seinfeld et al., 2016). These cloud microphysical properties can be influenced by the ambient aerosol conditions via the aerosol-cloud interaction (ACI), where clouds under regions that have relatively higher below-cloud aerosol concentrations exhibited reduced r_e, increased N_C, and enhanced both cloud liquid water contents and optical depths than the clouds under relatively clean regions (McComiskey et al., 2009; Chen et al., 2014). The MBL cloud microphysical properties changes induced by aerosols have been investigated from previous studies using in-situ measurements, ground- and satellite-based observations, and model simulations in multiple oceanic areas such as the eastern Pacific and eastern Atlantic (Twohy et al., 2005; Lu et al., 2007; Hill et al., 2009; Costantino and Bréon, 2010; Mann et al., 2014; Dong et al., 2015; Diamond et al., 2018; Wang et al., 2020).

The assessments of ACI, in particular using ground-based remote sensing, are found to vary in terms of the quantitative values, which represent the different cloud susceptibilities to aerosol loadings. Owing to the numerous approaches in assessing the ACI, such as the spatial and temporal scales, N_c and r_e retrieval methods, and more importantly, the different aerosol proxies that used in the ACI quantification, different ACI results could be achieved. For example, the studies using total aerosol number concentration and aerosol scattering/extinction coefficients to represent the aerosol loadings would result in relatively lower ACI values (Pandithurai et al., 2009; Liu et al., 2016). This is primarily attributed to the inclusion of aerosol species with different abilities to activate, which is determined by their physicochemical properties, and thus will cause non-negligible uncertainties in capturing the information of aerosol intrusion to the cloud (Feingold et al. 2006; Logan et al., 2014). While some studies found relatively higher ACI values using cloud condensation nuclei (CCN) number concentration (N_{CCN}), presumably due to the fact that CCN represents the portion of aerosols that can be activated and possesses the potential ability to further grow into cloud droplets, this favorably yields a more straightforward

https://doi.org/10.5194/acp-2021-391
Preprint. Discussion started: 7 June 2021


Atmospheric Chemistry and Physics Discussions

assessment of ACI (McComiskey et al., 2009; Zheng et al., 2020). It is noteworthy that the ACI variations have been found to have both increasing and decreasing trends in response to changing environmental water availability (Martin et al., 2004; Kim et al., 2008; McComiskey et al., 2009; Pandithurai et al., 2009; Martin et al., 2011; Liu et al., 2016; Zheng et al., 2020). Although these contradicting results have been postulated due to multiple factors such as cloud adiabaticity, condensational growth, collision coalescence, and atmospheric thermodynamics and dynamics, the underlying mechanisms in altering the ACI and causing the uncertainties in the ACI assessments remain unclear, therefore, further studies are necessary (Fan et al., 2016; Feingold and McComiskey, 2016; Seinfeld et al., 2016).

In terms of the aerosol influence on the cloud properties, the roles of meteorological factors on cloud formation and development are not negligible and hence are being explored in this study. The large-scale thermodynamic variables of the lower troposphere are widely used, such as the lower tropospheric stability (LTS), where the higher LTS values are found to be associated with a relatively shallower and well-mixed marine boundary layer, and is prone to stratiform cloud formations with higher cloud fractions (Wood and Bretherton, 2006; Yue et al., 2011; Rosenfeld et al., 2019). In the cloud-topped marine boundary layer maintained by cloud-top radiative cooling, the buoyancy generations contribute most to the turbulence kinetic energy (TKE) production (Nicholls, 1984; Hogan et al., 2009), where the intensity of turbulence denotes the coupling of MBL clouds to the below-cloud boundary layer. In terms of the cloud droplet growing process, especially in a clean environment with low below-cloud N_{CCN}, the cloud droplets at the cloud base experience rapid growth via the diffusion of water vapor, and subsequently enter the regime of active coalescence process (Rosenfeld and Woodley, 2003; Martins et al., 2011). The intensive turbulence is effectively modulating the cloud droplet growth by strengthening the coalescence process and the cloud cycling (Feingold et al., 1996, 1999; Pawlowska et al., 2006). The environmental effects on the MBL cloud formation and development processes and cloud microphysical properties have been widely implemented and considered in climate modeling (Medeiros and Stevens, 2011; West et al., 2014; Zhang et al., 2016). Thus, it is important to provide observational constraints on the environmental effects. The assessment of ACI from the ground-based perspective highly relies on the sensitivities of cloud droplet number concentrations and size distribution spectra to the changing of below-cloud CCN loadings. Hence, it is a nontrivial task to study the relationship between the environmental effect and the MBL cloud microphysical responses.

The Eastern North Atlantic (ENA) is a remote oceanic region that features persistent but diverse subtropical MBL clouds, owing to complex meteorological influences from the semi-permanent Azores High and prevailing large-scale subsidence (Wood et al., 2015). The ENA has become a favorable region to study the aerosol indirect effects on MBL clouds under a relatively clean environment with occasional

https://doi.org/10.5194/acp-2021-391
Preprint. Discussion started: 7 June 2021


Atmospheric Chemistry and Physics Discussions

intrusions of long-range transport of continental air mass (Logan et al., 2014; Wang et al., 2020). The atmospheric radiation measurement (ARM) program established the ENA permanent observatory site on the northern edge of Graciosa Island, Azores, in 2013, which continuously provides comprehensive measurements of the atmosphere, radiation, cloud, and aerosol from ground-based observation instruments. In this study, we target the non-precipitating single-layer MBL stratus and stratocumulus clouds during the period between September 2016 and May 2018 and examine the role of thermodynamical and dynamical variables on ACIs. This study aims to enhance the understanding of ACI, particularly disentangling the environmental effect and reducing the uncertainty in quantifying the ACI when modeling aerosol influences on MBL clouds. The ground-based observations and retrievals, and the reanalysis are introduced in section 2. Section 3 describes the aerosol, cloud and meteorological properties, and the variations of cloud microphysical properties under different environmental regimes. Moreover, the ACIs under given water vapor conditions and the roles of environmental effect on ACI are discussed in Section 3. The conclusion of the key findings and the future work are presented in section 4.

2. Data and methods

2.1 Cloud and aerosol properties

The cloud boundaries at the ARM ENA site are primarily determined by the ARM Active Remotely-Sensed Cloud Locations (ARSCL) product, which is a combination of data detected by multiple active remote-sensing instruments, including the Ka-band ARM Zenith Radar (KAZR) and laser ceilometer. The KAZR has an operating frequency at 35 GHz and is sensitive in cloud detection with very minimum attenuation up to the cloud top height (Widener et al., 2012). The temporal and vertical resolutions of KAZR reflectivity are 4 seconds and 30 m, respectively. The ceilometer operates at 910 nm laser beam and its attenuated backscatter data can be converted to the cloud base height up to 7.7 km with an uncertainty of ~10 m (Morris, 2016). Combing both KAZR and ceilometer measurements, the cloud base and top heights can be identified accordingly. The single-layer low cloud is defined as having a cloud top height lower than 3 km, with no additional cloud layer in the atmosphere above (Xi et al., 2010).

The cloud microphysical properties are retrieved from a combination of ground-based observations, including KAZR, ceilometer, and microwave radiometer. The detailed retrieval methods and procedures are described in Wu et al. (2020a). The retrieved cloud microphysical properties, both in time series and vertical profiles, have been validated using the collocated aircraft in-situ measurements during the Aerosol and Cloud Experiments in the Eastern North Atlantic field campaign (ACE-ENA). The retrieval

https://doi.org/10.5194/acp-2021-391
Preprint. Discussion started: 7 June 2021


Atmospheric Chemistry and Physics Discussions

uncertainties are estimated to be ~15% for cloud droplet effective radius (r_e) and ~35% for cloud droplet number concentration (N_c) (Wu et al., 2020a).

The surface cloud condensation nuclei (CCN) number concentrations (N_{CCN}) are measured by the CCN-100 (single-column) counter. Since the supersaturation (SS) levels are set to cycling between 0.10% and 1.10% approximately within one hour, N_{CCN} under a relatively stable supersaturation level has to be carefully calculated to rule out the impact of supersaturation on N_{CCN}. This study adopts the interpolation method given by $N_{CCN} = cSS^k$ (Twomey, 1959), where parameters c and k are fitted by a power-law function for every periodic cycle. In this study, the supersaturation level of 0.2% is used because it represents typical supersaturation conditions of boundary-layer stratiform clouds (Hudson and Noble, 2013; Logan et al., 2014; Wood et al., 2015; Siebert et al., 2021), and N_{CCN} at 0.2% supersaturation (hereafter $N_{CCN,0.2\%}$) is interpolated to 5-min temporal resolution.

2.2 Environmental conditions and cloud case selections

The integrated precipitable water vapor (PWV) is obtained from a 3-channel microwave radiometer (MWR3C), which operates at three frequency channels of 23.834, 30, and 89 GHz. The uncertainty of PWV is estimated to be ~0.03 cm (Cadeddu et al., 2013). The LTS parameter is used as a proxy of large-scale thermodynamic structure and is defined as the difference between the potential temperature at 700 hPa and surface ($\theta_{700} - \theta_{sfc}$). The LTS values are calculated from European Centre for Medium-Range Weather Forecasts (ECMWF) model outputs of potential temperature, by averaging over a grid box of 0.56°×0.56° centered at the ENA site. To match the temporal resolutions of the other variables, the original 1-hour LTS data are downscaled to 5-min under the assumption that the large-scale forcing would not have significant changes within an hour.

As for the boundary layer dynamics, the higher-order moments of vertical velocity are widely used in different model parameterization practices, such as higher-order turbulence closure and probability density function methods (Lappen and Randall, 2001; Zhu and Zuidema, 2009; Ghate et al., 2010). The vertical velocity variance can be used to represent the turbulence intensity in the below-cloud boundary layer (Feingold et al., 1999). In this study, the mean vertical component of the turbulence kinetic energy (TKE_w) are used, which is defined as:

$$TKE_w = \frac{1}{2}\overline{(w')^2}\,, \quad (1)$$

where the $(w')^2$ is the variance of vertical velocity measured from Doppler lidar with the noise correction applied to reduce the uncertainty to ~10% (Hogan et al., 2009; Pearson et al., 2009). The original Doppler lidar vertical velocity has a temporal resolution of 10-min (Newson et al., 2019), and it is further downscaled to 5-min for the temporal collocation purpose.

https://doi.org/10.5194/acp-2021-391
Preprint. Discussion started: 7 June 2021


Atmospheric Chemistry and Physics Discussions

In this study, the non-precipitating cloud periods are determined when the KAZR reflectivity at the ceilometer-detected cloud base height range does not exceed -37 dBZ (Wu et al., 2015, 2020b), which extensively rules out the wet-scavenging depletion on below-cloud CCN (Wood, 2006) and ensures the accuracy in capturing the below-cloud CCN loadings. Both retrieved cloud microphysical properties and CCN data are available from September 2016 to May 2018 and confine this period in this study.

3. Result and Discussion

3.1 Aerosol, cloud, and meteorological properties of selected cloud cases

A total of 20 non-precipitating cloud cases are selected to conduct this study, with the detailed time periods listed in Table 1, including 1143 samples in temporal resolution of 5-min, which corresponds to ~95 hours. Among the selected cases, there are three, eight, five, and four cases for Spring, Summer, Fall, and Winter seasons, respectively. MBL clouds often produce precipitation in the form of drizzle (Wood 2012, Wu et al., 2015, 2020b). A recent study of the seasonal variation of the drizzling frequencies (Wu et al., 2020b) showed that the MBL clouds in cold months (Oct-Mar) have the highest drizzling frequency of the year (~70%), while the clouds in warm months (Apr-Sept) are found to have a lower chance of drizzling (~45%). Therefore, the selection of a non-precipitating single-layer low cloud case that lasts at least 2 hours is limited, with only 6 cases found in the cold months and 14 cases found during the warm months.

The distributions of the aerosol and cloud properties, and the environmental conditions for the selected cases are shown in Fig. 1. The $N_{CCN,0.2\%}$ presents a normal distribution with a mean value of 215 cm^{-3} and median value of 217 cm^{-3}. About 97% of the $N_{CCN,0.2\%}$ samples lay below 350 cm^{-3} and represents a relatively clean environment (Logan et al., 2014, 2018). A few instances of aerosol intrusions (~3%) with higher $N_{CCN,0.2\%}$ were likely a result of continental air mass transport from North America (Logan et al., 2014; Wang et al., 2020). As for the cloud microphysical properties, the cloud-layer mean N_c and r_e (Fig. 1b and 1c) are also both normally distributed with median values close to the mean values. The majority of the N_c values (~91%) are lower than 125 cm^{-3} with a mean value of 86 cm^{-3}, and the r_e distribution peaks at 9 - 11 μm with a mean value of 10.1 μm. Both N_c and r_e values fall in the typical ranges of the non-precipitating MBL cloud characteristics over the ENA site (Dong et al., 2014; Wu et al., 2020b).

For all selected cases, the LTS, which represents the large-scale thermodynamic structure, is distributed bimodally across the range from 14K to 23K with mean and median values of 19.1K in Fig. 1d. A higher LTS magnitude represents a relatively stable environment and is favorable to the formation

https://doi.org/10.5194/acp-2021-391
Preprint. Discussion started: 7 June 2021


Atmospheric Chemistry and Physics Discussions

of marine stratocumulus (Medeiros and Stevens, 2011; Gryspeerdt et al., 2016). Leveraging the demarcation line at 19.1K may provide an opportunity to investigate the aerosol-cloud relationships under contrasting thermodynamic regimes. As an indicator of the below-cloud boundary layer turbulence, the TKE_w values present a gamma distribution that highly skewed to the right (Fig. 1e), with a mean value of 0.11 and a median value of 0.08 m^2s^{-2}. About half of the cloud samples are under relatively less turbulent environment, which suggests the weak connections between the cloud layer and the below-cloud boundary layer. The other half of the cloud samples, with relatively higher TKE_w values up to 0.4 m^2/s^2, imply tighter connections between cloud microphysical properties and below-cloud boundary layer accompanied by intensive turbulent conditions, which is favorable to enhance cloud droplet growth (Albrecht et al., 1995; Hogan et al., 2009; Ghate et al., 2010; West et al., 2014; Ghate and Cadeddu, 2019).

It is noteworthy that PWV values exhibit a bimodal distribution with a median value of 2.4 cm (Fig. 1f). About 43% of the samples have their PWV values in the range of 1.0 - 2.0 cm with the first peak in 1.2 - 1.6 cm, and 56% of the samples have PWV values higher than 2.2 cm with a second peak in 2.4 - 2.8 cm, which may be due to the seasonal difference of the selected cases. Fig. S1 shows the seasonal variation of the PWV from 2016 to 2018 when single-layer low clouds present. The monthly PWV values are as low as ~ 1.7 mm and remain nearly invariant from January through March, then monotonically increase up to ~ 3.4 cm (doubled) in August, and finally decrease dramatically to December. The selected cloud cases are distributed across the seasons with ~34% of the samples occurring during the months with the lowest mean PWV (Jan-Mar), while ~43% of the samples fall in the highest PWV months (Jun-Sept). These two obvious PWV regions will provide a great opportunity for us to further examine the ACI under different water vapor conditions.

3.2 Dependent of cloud microphysical properties on CCN and PWV

Figure 2 shows the cloud microphysical properties as a function of $N_{CCN,0.2\%}$ and PWV for the samples from 20 selected cases. As illustrated in Fig. 2a, there is a statistically significant positive correlation (R^2=0.9) between $ln(N_c)$ and $\ln(N_{CCN,0.2\%})$. The linear fit of $ln(N_c)$ to $\ln(N_{CCN,0.2\%})$ is then mathematically transformed to a power-law fitting function of N_c to $N_{CCN,0.2\%}$, and plotted as dash lines in Fig. 2a. The power-law fitting indicates that 90% of the variation in binned $ln(N_c)$ can be explained by the change in the binned $ln(N_{CCN,0.2\%})$ and further suggests that with more available below-cloud CCN, higher number concentrations are expected. The logarithmic ratio $\partial ln(N_c)/\partial ln(N_{CCN,0.2\%})$ is computed to be 0.44 from our study. This ratio is very close to 0.48 found by McComiskey et al. (2009),

https://doi.org/10.5194/acp-2021-391
Preprint. Discussion started: 7 June 2021


Atmospheric Chemistry and Physics Discussions

who also used ground-based measurements to study the marine stratus clouds over the California coast. The logarithmic ratio (0.44) is also close to the result (0.458) of Lu et al. (2007) who used aircraft in-situ measured cloud droplet and accumulation mode aerosol number concentration for the marine stratus and stratocumulus clouds over the eastern Pacific Ocean. Our result agrees well with previous studies on the relationship between cloud droplet and CCN in MBL clouds, which elaborate the bulk microphysical responses of N_c to $N_{CCN,0.2\%}$ over different marine locations.

The PWV values are represented as blue circles (larger one for higher PWV) in Fig. 2a in order to study the role of water vapor availability on the CCN-N_c conversion process. As demonstrated in Fig. 2a, the PWV values almost mimic the increasing $N_{CCN,0.2\%}$ trend, which is also governed by the seasonal $N_{CCN,0.2\%}$ and the selected cloud cases. Fig. S2 shows the seasonal variation of $N_{CCN,0.2\%}$ from 2016 to 2018. It is noticeable that the monthly $N_{CCN,0.2\%}$ values, which mimic the monthly variation of PWV, are much higher during warm months (May-Oct) than during cold months (Nov-Apr). This seasonal $N_{CCN,0.2\%}$ variation is also found in recent studies of MBL aerosol composition and number concentration. During the warm months, the below-cloud boundary layer is enriched by the accumulation mode of sulfate and organic particles via local generation and long-range transport induced by the semi-permanent Azores High, which are found to be hydrophilic and can be great CCN contributors (Wang et al., 2020; Zawadowicz et al., 2020; Zheng et al., 2018, 2020). Therefore, the coincidence of high $N_{CCN,0.2\%}$ and PWV does not necessarily imply a physical relationship, but instead is the result of their similar seasonal trend. When taking the PWV into account, R^2 increases from 0.9 to 0.98, and this new relationship suggests that the covariability between the binned $ln(N_{CCN,0.2\%})$ and ln (PWV) can explain 98% of the change in binned $ln(N_c)$. Intuitively, if the CCN-N_c relationship is primarily dominated by the diffusion of water vapor, more CCN and higher PWV should result in a continuously increasing of N_c. However, the rapid increase of N_c (37 to 92 cm^{-3}) in the first half of $N_{CCN,0.2\%}$ bins (<250 cm^{-3}) does not happen in the second half of the $N_{CCN,0.2\%}$ bins (>250 cm^{-3}) where the slope of N_c increase (96 to 103 cm^{-3}) appears to be flattened for higher $N_{CCN,0.2\%}$ and PWV bins. Furthermore, the joint power-law fitting of N_c (to $N_{CCN,0.2\%}$ and PWV) appears to be constantly lower than the single power-law fitting of N_c (to $N_{CCN,0.2\%}$ solely) in each bin. The negative power of PWV in this relationship suggests that PWV might play a stabilization role in the diffusional growth process, which will be further analyzed in the following sections.

The relationship between r_e and $N_{CCN,0.2\%}$ is shown in Fig. 2b where there is no significant relationship between r_e with $N_{CCN,0.2\%}$ solely, given a near-zero slope and the low correlation coefficient (fitted line not plotted). However, after applying a multiple linear regression to the logarithmic form of

https://doi.org/10.5194/acp-2021-391
Preprint. Discussion started: 7 June 2021


Atmospheric Chemistry and Physics Discussions

r_e, $N_{CCN,0.2\%}$ and PWV, a significant correlation among those three variables is found. The r_e is negatively correlated with $N_{CCN,0.2\%}$ and positively correlated with PWV, and nearly 82% of the variations in binned ln (r_e) can be explained by the joint changes of the binned $ln(N_{CCN,0.2\%})$ and ln (PWV). This indicates that in the bulk part, the r_e decreases with increasing $N_{CCN,0.2\%}$ and enlarges with increasing PWV. Notice that in lower $N_{CCN,0.2\%}$ bins (<150 cm^{-3}) where the PWV values are the lowest among all the bins (1.33 - 1.69 cm), the limitation of cloud droplet growth by competing for the available water vapor is evident by the changes in N_c and r_e. For example, the $N_{CCN,0.2\%}$ changes from 47 to 128 cm^{-3}, the N_c increases from 37 to 71 cm^{-3} and r_e only increases from 9.30 to 9.74 μm. In other words, nearly tripling the CCN loading leads to roughly doubling N_c, while the r_e is only enlarged by 0.44 μm (4.7%). In the relatively low available PWV regime, it is clear that even with more CCN being converted into cloud droplets, the limited water vapor condition prohibits the further diffusional growth of those cloud droplets. However, in the higher $N_{CCN,0.2\%}$ bins (>150 cm^{-3}) with relatively higher PWV, the binned r_e values fluctuate and decrease with increasing CCN bins under similar PWV (i.e., the two $N_{CCN,0.2\%}$ ranges from 200-400 cm^{-3}, and from 400-500 cm^{-3}). Since r_e essentially represents the area-weighted information of the cloud droplet size distribution (DSD), this sorting method of r_e inevitably entangles multiple cloud droplet evolution processes and environmental effects that can alter the DSD, especially under the condition of sufficient water supply. Therefore, the further assessment of the r_e responses to the $N_{CCN,0.2\%}$ loading under the constraints of water vapor should be discussed in order to untangle the impacts of different processes and environmental effects on r_e.

3.3 The role of adiabaticity in cloud microphysical variation

Following the discussion on the potential coalescence process in the last section, the cloud adiabaticity conditions for the selected cases are investigated in this section. The profiles of cloud r_e and LWC are plotted in normalized height from cloud base (z_b) to cloud top height (z_t) (Fig. 3), which is given by $z_n = (z - z_b) / (z_t - z_b)$. The solid lines denote the mean values, and the shaded area represents one standard deviation at each normalized height z_n. The normalized r_e increases from ~8.6 μm at the cloud base toward ~11 μm near the upper part of the cloud where z_n is 0.7, primarily through condensational growth and coalescence processes, and then decreases toward the cloud top due to cloud-top entrainment. Profiles of retrieved LWC and calculated adiabatic LWC_{ad} (blue line) are presented in Fig. 4b where $LWC_{ad(z)} = \Gamma_{ad}(z - z_b)$, and Γ_{ad} denotes the linear increase of LWC with height under an ideal adiabatic condition (Wood, 2005). The LWC_{ad} is computed using an interpolated sounding, following the method of Wu et al. (2020b), and the adiabaticity (f_{ad}) can be described as the ratio of

https://doi.org/10.5194/acp-2021-391
Preprint. Discussion started: 7 June 2021


Atmospheric Chemistry and Physics Discussions

LWC to LWC_{ad}. As demonstrated in Fig. 3b, the f_{ad} values, which is the ratio of LWC to LWC_{ad}, reach a maximum of 0.8 at the cloud base and a minimum of 0.38 at the cloud top. In the sub-adiabatic cloud regime, the decrease of f_{ad} is largely due to the cloud-top entrainment and coalescence processes even in the non-precipitating MBL clouds (Wood, 2012; Braun et al., 2018; Wu et al. 2020b). To better understand the implication of cloud adiabaticity with respect to CCN-N_c conversion, all of the f_{ad} samples are separated into two groups by the median value of the layer-mean f_{ad} (0.61). The N_c is plotted against the binned $N_{CCN,0.2\%}$ (Fig. 4) for the near-adiabatic regime (f_{ad} > 0.61) and sub-adiabatic regime (f_{ad} < 0.61). For the near-adiabatic regime, N_c increases from ~60 cm^{-3} to 119 cm^{-3} with increased $N_{CCN,0.2\%}$ and PWV, and the $N_{CCN,0.2\%}$ and PWV appear to play equally important roles in terms of the N_c increase. The result is as expected because the process of condensational growth is predominant in the near-adiabatic cloud, that is, with increasing water vapor supply, the higher CCN loading can effectively lead to more cloud droplets. However, in the sub-adiabatic cloud regime, N_c increases with increased $N_{CCN,0.2\%}$ but possesses a negative correlation with PWV, which results in a slow increase of N_c. The mean reduction of N_c in the sub-adiabatic regime is computed to be ~33% compared to that for the near-adiabatic cloud. As previously studied, the coalescence process contributes significantly to N_c depletion, even in a non-precipitating marine boundary cloud (Feingold et al., 1996; Wood, 2006). Thus, the lower N_c in the sub-adiabatic regime may be partly due to the combined effect of coalescence and entrainment (Wood, 2006; Hill et al., 2009; Yum et al., 2015; Wang et al., 2020). The impact of cloud adiabaticities on CCN-N_c conversions may shed light on interpreting the aerosol-cloud interaction under different environmental effects.

3.4 Aerosol-cloud interaction under different PWV

As previously discussed above and suggested by earlier studies, the conditions of water vapor supply have a substantial impact on various processes from CCN-N_c conversion to in-cloud droplet condensational growth and coalescence, hence effectively altering the cloud DSD (Feingold et al., 2006; McComiskey et al., 2009; Zheng et al., 2020). Moving forward to examine how r_e responds to the changes of $N_{CCN,0.2\%}$ in the context of given water vapor availability, an index describing the aerosol-cloud interaction process is introduced as follows:

$$\mathrm{ACI_r} = -\left.\frac{\partial \ln(\mathrm{r_e})}{\partial \ln(N_{CCN,0.2\%})}\right|_{\mathrm{PWV}}. \quad (2)$$

The $\mathrm{ACI_r}$ represents the relative change of r_e with respect to the relative change of $N_{CCN,0.2\%}$, where positive $\mathrm{ACI_r}$ denotes the decrease of r_e with increased $N_{CCN,0.2\%}$ under binned PWV. This assessment

https://doi.org/10.5194/acp-2021-391
Preprint. Discussion started: 7 June 2021


Atmospheric Chemistry and Physics Discussions

of ACI_r focuses on the relative sensitivity of the cloud microphysics response in the water vapor stratified environment (Twomey, 1977; Feingold et al., 2003; Garrett et al., 2004). Fig. 5 shows the variation of ACI_r under different PWV bins, and illustrates the calculation of ACI_r in three different PWV ranges. Note that in Fig. 5b, the regressions are derived from all points (statistically significant with a confidence level of 95%) except for one point at PWV=2.0 cm. As shown in Fig. 5b, the ACI_r values range from close-to-zero values (-0.004) to 0.207, with the mean value of 0.096 ± 0.026. The ACI_r range of this study agrees well with the previous studies of MBL cloud aerosol-cloud interactions (McComiskey et al., 2009; Pandithurai et al., 2009; Liu et al., 2016). It is noteworthy that the variation of ACI_r with PWV suggests two different relationships under separated PWV conditions, as discussed in the following two paragraphs.

Under the relatively lower PWV condition (<2.0 cm), the low values of ACI_r (-0.004 - 0.074) indicate that r_e is less sensitive to $N_{CCN,0.2\%}$, and the dependence on PWV is also insignificant given by the flat regression line (green dash line) and low correlation coefficient of 0.17 (Fig. 5b). As discussed in section 3.2, the limited water vapor can weaken the ability of condensational growth of the cloud droplet converted from CCN, that is, the increase of CCN loading cannot be effectively reflected by a decrease in r_e. For example, a near quadruple increase of $N_{CCN,0.2\%}$ only leads to a 41% decrease in r_e in the PWV range of 1.2-1.4 cm as shown in Fig. 5a. So that in this regime, even with a slight PWV increase, the lack of a sufficient amount of large cloud droplets is favorable to the predominant condensational growth process, which effectively narrows the cloud DSD and, in turn, confines the variable range of r_e with respect to $N_{CCN,0.2\%}$ (Pawlowska et al., 2006; Zheng et al., 2020). In this situation, the abilities of CCN to cloud droplet conversion and the droplet condensational growth are limited by the insufficient water vapor, rather than an influx of CCN.

However, under the relatively higher PWV regime (>2.2 cm), the ACI_r values become more positive and express a significant increasing trend with PWV (correlation coefficient of 0.95), which indicates that r_e is more susceptible to $N_{CCN,0.2\%}$ in this regime. On the one hand, due to the sufficient water vapor supply, the enhanced condensational growth process allows more CCN to grow into cloud droplets, so that the limiting factor of the droplet growth corresponds to the changes in CCN loading. On the other hand, the increased N_c values associated with higher water vapor supply in the cloud effectively enhance the coalescence process. This results in broadening the cloud DSD and increasing the variation range of r_e in response to the changes of $N_{CCN,0.2\%}$. To test our hypothesis of active coalescence under higher water vapor conditions, Table 2 lists the occurrence frequencies of large r_e values (> 12 and 14 μm) under the six high PWV bins (2.2 – 3.4 cm), because this range of 12-14 μm can serve as the critical

https://doi.org/10.5194/acp-2021-391
Preprint. Discussion started: 7 June 2021


Atmospheric Chemistry and Physics Discussions

demarcation of an efficient coalescence process (Gerber, 1996; Freud and Rosenfeld, 2012; Rosenfeld et al., 2012). As listed in Table 2, for the six high PWV bins, the occurrence frequencies of r_e>12 μm are 22.4%, 32.0%, 51.2%, 70.1%, 96.5% and 95.1%, and the occurrence frequencies of r_e>14 μm are 1.72%, 2.41%, 4.35%, 16.4%, 35.1% and 9.76%, respectively.

The increasing trends of large r_e occurrences mimic the trend of $\mathrm{ACI_r}$ and suggest that with increased PWV, cloud droplets have a greater chance to grow via the effective coalescence process and subsequently lead to an enlargement of $\mathrm{ACI_r}$. Although previous studies have brought up the potential impacts of cloud droplet coalescence process on ACI, it is rarely seen that the relationship among them has been discussed in detail. Here we provide possible explanations on how the enhanced coalescence process can enlarge $\mathrm{ACI_r}$. Quantitatively, $\mathrm{ACI_r}$ is described by the log partial derivative ratio of r_e to $N_{CCN,0.2\%}$, thus a sharper decrease of r_e with respect to a given $N_{CCN,0.2\%}$ range can result in a steeper slope and in turn, larger $\mathrm{ACI_r}$ (i.e., a $N_{CCN,0.2\%}$ increase of 49% leads to a r_e decrease of 41% in the 2.8-3.0 cm bin in Fig. 5a). Physically, this relies on how the cloud droplet size distribution spectra would change with different CCN loadings. Therefore, particularly in low CCN conditions, sufficient water vapor availability allows cloud droplets to continuously grow via diffusion of water vapor (i.e., condensational growth), and enter the active cloud-droplet coalescence regime. In contrast, the increase in cloud droplets can effectively reduce N_c via the process of large cloud droplets collecting small droplets, and small droplets coalescing into large droplets. Consequently, the size distribution spectra are effectively broadened toward the large tail by the coalescence, so that r_e is enlarged. With more CCN available, the size distribution spectra are narrowed by the enhanced condensational growth and regress toward the small tail by increasing the amount of newly converted cloud droplets and result in decreased r_e. These interactions between CCNs and cloud droplets ultimately result in the broadened changeable range of r_e, and in turn, the enlarged $\mathrm{ACI_r}$.

3.5 Impacts of meteorological factors on ACI

3.5.1 The role of lower tropospheric thermodynamics

The LTS parameter is used to infer the large-scale thermodynamic structures for the selected cases in order to examine their impacts on ACI. The samples are separated into two regimes: high LTS and low LTS using the median LTS value (19.1K) as a threshold. The N_c values for the high LTS regime are generally higher than those in the low LTS region (Fig. S3), though their difference is only 4.7%. Since LTS is calculated by the difference between free tropospheric and surface potential temperatures, a high LTS value represents a strong temperature inversion that caps the boundary layer, and implies a

https://doi.org/10.5194/acp-2021-391
Preprint. Discussion started: 7 June 2021


Atmospheric Chemistry and Physics Discussions

thin entrainment zone that restricts the effectiveness of the cloud-top entrainment. Moreover, a more stable lower troposphere is prone to boundary layer cloud formation with a lower cloud base height and accompanies a well-mixed boundary layer that couple the surface moisture and aloft (Klein and Hartmann, 1993; Wood and Bretherton, 2006; Wood, 2012). Thus, the high LTS values are often found to be associated with clouds that more close to adiabatic (Kim et al., 2008), which results in more N_c with less depletion.

To examine the impact of LTS on the water constrained $\mathrm{ACI_r}$, the samples are further separated by the median PWV (2.4 cm) and median LTS, so each regime has ~25% of the total samples. As shown in Fig. 6, where the regression lines for the four regimes are fitted to the 95% confidence interval, the $\mathrm{ACI_r}$ differences between low and high PWV regimes are still retained. In the low PWV regime, the $\mathrm{ACI_r}$ values are limited to 0.03 and 0.053 for low and high LTS regimes, respectively. In the high PWV regime, the $\mathrm{ACI_r}$ values are 0.154 and 0.171 for low and high LTS regimes, respectively, which is about 3-5 times greater than those in low PWV regime. It appears that PWV plays a more important role in $\mathrm{ACI_r}$ than LTS since the LTS is mostly capturing the large-scale thermodynamical structures, and is obtained from a coarser temporal resolution. Thus, the LTS does not essentially have strict correspondence to the strength of boundary layer turbulence (which more directly interferes with the cloud processes). LTS may not effectively represent the connection between cloud layer and boundary layer CCN and moisture in terms of both spatial and temporal scales, and thus induces limitations in assessing the role of thermodynamics on the $\mathrm{ACI_r}$.

3.5.2 The role of boundary layer turbulence

To examine the role of the dynamical factors on ACI, the $\mathrm{TKE_w}$ parameter is used to represent the intensity of below-cloud boundary layer turbulence. The median $\mathrm{TKE_w}$ ($0.08\ \mathrm{m^2 s^{-2}}$) is used to separate the N_c variation with $N_{CCN,0.2\%}$ for low and high $\mathrm{TKE_w}$ regimes (Fig. S4). The N_c values are higher (with a mean increase of 20%) under high $\mathrm{TKE_w}$ environments than those under lower $\mathrm{TKE_w}$, across all CCN bins. The higher logarithmic ratios of N_c to PWV for high $\mathrm{TKE_w}$ regime suggest a more sensitive N_c response to CCN with an increased water vapor supply. This is mainly due to a closer connection between the CCN below and the cloud layer loft, accompanied by stronger boundary layer turbulence, so that more CCN can be converted into cloud droplets. When using the mean values of 215 $\mathrm{cm^{-3}}$ for $N_{CCN,0.2\%}$ and 2.2 cm for PWV as an example, the calculated N_c values from the multiple regressions are 83 and 68 $\mathrm{cm^{-3}}$ for high and low $\mathrm{TKE_w}$ regimes, respectively. Thus, under the condition

https://doi.org/10.5194/acp-2021-391
Preprint. Discussion started: 7 June 2021


Atmospheric Chemistry and Physics Discussions

417 at given $N_{CCN,0.2\%}$ and PWV, the boundary layer with strengthened turbulence would be favorable for
418 more cloud droplets to be converted from CCN by water vapor condensation.
419 Similar to the aforementioned data separation method, the samples are further separated into four
420 regimes demarcated by PWV and TKE_w in Fig. 7. Similar to the results in Fig. 6, the ACI_r values in the
421 higher PWV regime are also much higher than those in the lower PWV no matter low or high TKE_w
422 regimes, whereas TKE_w plays a more important role in ACI_r than LTS because the ACI_r values in the
423 high TKE_w regime are double those in the low TKE_w regime. In the regimes of higher TKE_w and PWV,
424 r_e is highly sensitive to the CCN loading with the highest ACI_r of 0.252. The sufficient water vapor
425 availability allows CCN to be converted into cloud droplets more effectively, while the relatively higher
426 TKE_w indicates stronger turbulence in the below-cloud boundary layer. The CCN and moisture below-
427 cloud layer are efficiently transported and mixed aloft via the ascending branch of the eddies (Nicholls,
428 1984; Hogan et al., 2009), hence effectively connected to the cloud layer. Therefore, under the lower
429 CCN loading condition, the active coalescence process results in the depletion of small cloud droplets
430 and broadening of cloud DSD (Chandrakar et al., 2016), which leads to further enlarged r_e. However,
431 with higher CCN intrusion into the cloud layer, the enhanced cloud droplet conversion and the
432 subsequential condensational growth behave contradictorily to narrows the DSD (Pinsky and Khain,
433 2002; Pawlowska et al., 2006), which leads to decreased r_e. Therefore, the MBL clouds are distinctly
434 susceptible to CCN loading under the environments of sufficient water vapor and strong turbulence in
435 which the ACI_r is enlarged.
436 Under high PWV but low TKE_w conditions, the mean ACI_r reduces to 0.125 (~ 50% of that under
437 high TKE_w). The weaker turbulence loosens the connection between cloud layer and the underlying
438 boundary layer, results in a less effective conversion of CCN into cloud droplets, and then diminishes
439 the r_e sensitivity to CCN. Although the constraints of insufficient water vapor on the ACI_r are still
440 evident, the ACI_r value is doubled from 0.017 in low TKE_w regime to 0.035 in high TKE_w regime. The
441 ACI_r differences between the two TKE_w regimes attest that ACI_r strongly depends on the connection
442 between the cloud layer and the boundary layer CCN and moisture, that is, strong turbulence can enhance
443 the susceptibility of r_e to CCN. Given the significant increase of ACI_r, the TKE_w demarcation line of
444 0.08 m^2s^{-2}, which corresponds to the mean vertical velocity variation of 0.16 m^2s^{-2}, may be a feasible
445 way to distinguish the impact of turbulence effect on the cloud microphysical responses to the change in
446 CCN loadings.
447 In this study, the relationship between turbulence and ACI is found to be valid in non-precipitating
448 marine boundary-layer clouds. Theoretically, the effect of turbulence on ACI_r would appear to be

https://doi.org/10.5194/acp-2021-391
Preprint. Discussion started: 7 June 2021


Atmospheric Chemistry and Physics Discussions

449 artificially amplified, if in the presence of precipitation. The intensive turbulence can enhance the
450 coalescence process and accelerate the CCN-cloud cycling, and subsequently, the CCN depletion due to
451 precipitation and coalescence scavenging would result in quantitatively enlarged ACI_r (Feingold et al.,
452 1996, 1999; Duong et al., 2011; Braun et al., 2018). Though it is beyond the slope of this study, it would
453 be of interest to perform such analysis on the aerosol-cloud-precipitation interaction using ground-based
454 remote sensing in the future study.
455
456 **4. Summaries and Conclusions**

457 Over the ARM-ENA site, a total of 20 non-precipitating single-layer MBL stratus and stratocumulus
458 cloud cases are selected in order to investigate the aerosol-cloud interaction (ACI). The distributions of
459 CCN and cloud properties for selected cases represent the typical characteristics of non-precipitating
460 MBL clouds in the relatively clean environment over the remote oceanic area. The impact of different
461 environmental effects on ACI is analyzed.
462 The overall variations of N_c with $N_{CCN,0.2\%}$ show an increasing trend, regardless of the water vapor
463 condition, while the sufficient PWV appears to stabilize the CCN-N_c conversion process. The water
464 vapor limitation on cloud droplet growth is evident in the lower $N_{CCN,0.2\%}$ up to 150 cm^{-3} with low PWV
465 values, where a near tripling of CCN loading leads to a near doubling of N_c but only 4.7% increase in r_e.
466 When $N_{CCN,0.2\%}$ is greater than 250 cm^{-3} and PWV values are also relatively high, r_e appears to
467 decrease with increasing $N_{CCN,0.2\%}$ under similar water vapor conditions. In a more adiabatic cloud
468 vertical structure, the cloud droplet is dominated by condensational growth, so N_c responses to increased
469 $N_{CCN,0.2\%}$ and PWV are strengthened. When the cloud layer become more sub-adiabatic, the effect of
470 coalescence leads to the depletion of N_c and thus, the competition between the condensational growth
471 and coalescence processes has a strong impact on the variations of cloud microphysics to CCN loading.
472 The ACI_r values vary from -0.004 to 0.207 for different PWV conditions where the ACI_r appears to
473 be diminished under limited water vapor availability due to the limited droplet activation and
474 condensational growth process. While under relatively sufficient water supply condition, r_e shows more
475 sensitive responses to the changes of $N_{CCN,0.2\%}$, due to the combined effect of condensational growth and
476 coalescence processes accompanying the higher N_c and PWV. The coalescence process further enlarges
477 r_e, particularly in low CCN loading, while the enhanced condensational growth narrows the cloud DSD
478 and decreases r_e, so that a broader variable range of r_e with respect to $N_{CCN,0.2\%}$ change results in a
479 higher ACI_r value.

https://doi.org/10.5194/acp-2021-391
Preprint. Discussion started: 7 June 2021


Atmospheric Chemistry and Physics Discussions

To investigate the impacts of environmental effect on the ACI_r, the LTS parameter is used as a proxy of the thermodynamic structure. A higher LTS regime is favorable to the adiabatic cloud with lower cloud base height, accompanied by a well-mixed boundary layer, which likely enhances the cloud microphysical responses to CCN loadings. However, the ACI_r in different LTS regimes cannot be distinctly differentiated, partly due to the competing effect of adiabaticities and turbulence characteristics on the cloud droplet development processes.

In contrast, the intensity of boundary layer turbulence, which is represented by TKE_w, plays a more important role in ACI_r than LTS. The N_c shows more sensitive response to CCN with increased water vapor supply for the higher TKE_w regime, which may be due to enhanced CCN to cloud droplet conversion induced by intensive boundary layer turbulence. As for ACI_r, assessments in different TKE_w and PWV regimes, the constraints of insufficient water vapor on the ACI_r are still evident, but in both PWV regimes the ACI_r values increase more than double when going from low TKE_w to high TKE_w regimes. Noticeably, the ACI_r increases from 0.125 in low TKE_w regime to 0.252 in high TKE_w regime, under high PWV conditions. The intensive below-cloud boundary layer turbulence strengthens the connection between the cloud layer and below-cloud CCN and moisture. So that with sufficient water vapor, an active coalescence leads to further enlarged r_e, particularly for low CCN loading condition, while the enhanced N_c from condensational growth induced by increased $N_{CCN,0.2\%}$ can effectively decrease r_e. Combining these processes together, the enlarged ACI_r is presented.

In this study, the non-precipitating MBL clouds are found to be most susceptible to the below-cloud CCN loading under environments with sufficient water vapor and stronger turbulence. And the TKE_w demarcation line of 0.08 m^2s^{-2} might be feasible in distinguishing the turbulence-enhanced aerosol-cloud interaction. Future studies will be focusing on exploring the role of environmental effects on the aerosol-cloud-precipitation interactions in MBL stratocumulus through an integrative analysis of observations and model simulations.

Data availability. Data used in this study can be accessed from the DOE ARM's Data Discovery at https://adc.arm.gov/discovery/

Author contributions. The original idea of this study is discussed by XZ, BX, and XD. XZ performed the analyses and wrote the manuscript. XZ, BX, XD and PW participated in further scientific discussion and provided substantial comments and edits on the paper.

https://doi.org/10.5194/acp-2021-391
Preprint. Discussion started: 7 June 2021

Atmospheric Chemistry and Physics Discussions

Competing interests. The authors declare that they have no conflict of interest.

Special issue statement. This article is part of the special issue "Marine aerosols, trace gases, and clouds over the North Atlantic (ACP/AMT inter-journal SI)". It is not associated with a conference.

Acknowledgments. The ground-based measurements were obtained from the Atmospheric Radiation Measurement (ARM) Program sponsored by the U.S. Department of Energy (DOE) Office of Energy Research, Office of Health and Environmental Research, and Environmental Sciences Division. The reanalysis data were obtained from the ECMWF model output, which provides explicitly for the analysis at the ARM ENA site. The data can be downloaded from https://adc.arm.gov/discovery/. This work was supported by the NSF grants AGS-1700728 and AGS-2031750, and also supported as part of the "Enabling Aerosol-cloud interactions at GLobal convection-permitting scalES (EAGLES)" project (74358), funded by the U.S. Department of Energy, Office of Science, Office of Biological and Environmental Research, Earth System Modeling program with the subcontract to the University of Arizona. A special thanks to Dr. Timothy Logan for the input and advice to improve this manuscript.

References.

Albrecht, B. A., Bretherton, C. S., Johnson, D., Schubert, W. H. and Frisch, A. S.: The Atlantic Stratocumulus Transition Experiment - ASTEX, Bull. - Am. Meteorol. Soc., doi:10.1175/1520-0477(1995)076<0889:TASTE>2.0.CO;2, 1995.

Braun, R. A., Dadashazar, H., MacDonald, A. B., Crosbie, E., Jonsson, H. H., Woods, R. K., Flagan, R. C., Seinfeld, J. H. and Sorooshian, A.: Cloud Adiabaticity and Its Relationship to Marine Stratocumulus Characteristics Over the Northeast Pacific Ocean, J. Geophys. Res. Atmos., doi:10.1029/2018JD029287, 2018.

Cadeddu, M. P., Liljegren, J. C. and Turner, D. D.: The atmospheric radiation measurement (ARM) program network of microwave radiometers: Instrumentation, data, and retrievals, Atmos. Meas. Tech., doi:10.5194/amt-6-2359-2013, 2013.

https://doi.org/10.5194/acp-2021-391
Preprint. Discussion started: 7 June 2021


Atmospheric Chemistry and Physics Discussions

541 Chandrakar, K. K., Cantrell, W., Chang, K., Ciochetto, D., Niedermeier, D., Ovchinnikov, M., Shaw, R.
542 A. and Yang, F.: Aerosol indirect effect from turbulence-induced broadening of cloud-droplet size
543 distributions, Proc. Natl. Acad. Sci. U. S. A., doi:10.1073/pnas.1612686113, 2016.
544 Chen, Y. C., Christensen, M. W., Stephens, G. L. and Seinfeld, J. H.: Satellite-based estimate of global
545 aerosol-cloud radiative forcing by marine warm clouds, Nat. Geosci., doi:10.1038/ngeo2214, 2014.
546 Costantino, L. and Bréon, F. M.: Analysis of aerosol-cloud interaction from multi-sensor satellite
547 observations, Geophys. Res. Lett., doi:10.1029/2009GL041828, 2010.
548 Diamond, M. S., Dobracki, A., Freitag, S., Griswold, J. D. S., Heikkila, A., Howell, S. G., Kacarab, M.
549 E., Podolske, J. R., Saide, P. E. and Wood, R.: Time-dependent entrainment of smoke presents an
550 observational challenge for assessing aerosol-cloud interactions over the southeast Atlantic Ocean,
551 Atmos. Chem. Phys., doi:10.5194/acp-18-14623-2018, 2018.
552 Dong, X., Xi, B., Kennedy, A., Minnis, P. and Wood, R.: A 19-month record of marine aerosol-cloud-
553 radiation properties derived from DOE ARM mobile facility deployment at the Azores. Part I: Cloud
554 fraction and single-layered MBL cloud properties, J. Clim., doi:10.1175/JCLI-D-13-00553.1, 2014.
555 Dong, X., Schwantes, A. C., Xi, B. and Wu, P.: Investigation of the marine boundary layer cloud and
556 CCN properties under coupled and decoupled conditions over the azores, J. Geophys. Res.,
557 doi:10.1002/2014JD022939, 2015.
558 Duong, H. T., Sorooshian, A. and Feingold, G.: Investigating potential biases in observed and modeled
559 metrics of aerosol-cloud-precipitation interactions, Atmos. Chem. Phys., doi:10.5194/acp-11-4027-
560 2011, 2011.
561 Feingold, G., Kreidenweis, S. M., Stevens, B. and Cotton, W. R.: Numerical simulations of stratocumulus
562 processing of cloud condensation nuclei through collision-coalescence, J. Geophys. Res. Atmos.,
563 doi:10.1029/96jd01552, 1996.

https://doi.org/10.5194/acp-2021-391
Preprint. Discussion started: 7 June 2021

564 Feingold, G., Frisch, A. S., Stevens, B. and Cotton, W. R.: On the relationship among cloud turbulence,
565 droplet formation and drizzle as viewed by Doppler radar, microwave radiometer and lidar, J.
566 Geophys. Res. Atmos., doi:10.1029/1999JD900482, 1999.
567 Feingold, G., Furrer, R., Pilewskie, P., Remer, L. A., Min, Q. and Jonsson, H.: Aerosol indirect effect
568 studies at Southern Great Plains during the May 2003 Intensive Operations Period, J. Geophys. Res.
569 Atmos., doi:10.1029/2004JD005648, 2006.
570 Feingold, G. and McComiskey, A.: ARM's Aerosol–Cloud–Precipitation Research (Aerosol Indirect
571 Effects), Meteorol. Monogr., doi:10.1175/amsmonographs-d-15-0022.1, 2016.
572 Freud, E. and Rosenfeld, D.: Linear relation between convective cloud drop number concentration and
573 depth for rain initiation, J. Geophys. Res. Atmos., doi:10.1029/2011JD016457, 2012.
574 Garrett, T. J., Zhao, C., Dong, X., Mace, G. G. and Hobbs, P. V.: Effects of varying aerosol regimes on
575 low-level Arctic stratus, Geophys. Res. Lett., doi:10.1029/2004GL019928, 2004.
576 Gerber, H.: Microphysics of marine stratocumulus clouds with two drizzle modes, J. Atmos. Sci.,
577 doi:10.1175/1520-0469(1996)053<1649:MOMSCW>2.0.CO;2, 1996.
578 Ghate, V. P., Albrecht, B. A. and Kollias, P.: Vertical velocity structure of nonprecipitating continental
579 boundary layer stratocumulus clouds, J. Geophys. Res. Atmos., doi:10.1029/2009JD013091, 2010.
580 Ghate, V. P. and Cadeddu, M. P.: Drizzle and Turbulence Below Closed Cellular Marine Stratocumulus
581 Clouds, J. Geophys. Res. Atmos., doi:10.1029/2018JD030141, 2019.
582 Gryspeerdt, E., Quaas, J. and Bellouin, N.: Constraining the aerosol influence on cloud fraction, J.
583 Geophys. Res., doi:10.1002/2015JD023744, 2016.
584 Hill, A. A., Feingold, G. and Jiang, H.: The influence of entrainment and mixing assumption on aerosol–
585 cloud interactions in marine stratocumulus, J. Atmos. Sci., doi: 10.1175/2008JAS2909.1, 2009.
586 Hogan, R. J., Grant, A. L. M., Illingworth, A. J., Pearson, G. N. and O'Connor, E. J.: Vertical velocity
587 variance and skewness in clear and cloud-topped boundary layers as revealed by Doppler lidar, Q.
588 J. R. Meteorol. Soc., doi:10.1002/qj.413, 2009.

https://doi.org/10.5194/acp-2021-391
Preprint. Discussion started: 7 June 2021

589 Hudson, J. G. and Noble, S.: CCN and Vertical Velocity Influences on Droplet Concentrations and
590 Supersaturations in Clean and Polluted Stratus Clouds, J. Atmos. Sci., doi:10.1175/jas-d-13-086.1,
591 2013.
592 Klein, S. A. and Hartmann, D. L.: The seasonal cycle of low stratiform clouds, J. Clim.,
593 doi:10.1175/1520-0442(1993)006<1587:TSCOLS>2.0.CO;2, 1993.
594 Kim, B. G., Miller, M. A., Schwartz, S. E., Liu, Y. and Min, Q.: The role of adiabaticity in the aerosol
595 first indirect effect, J. Geophys. Res. Atmos., doi:10.1029/2007JD008961, 2008.
596 Liu, J., Li, Z. and Cribb, M.: Response of marine boundary layer cloud properties to aerosol perturbations
597 associated with meteorological conditions from the 19-month AMF-Azores campaign, J. Atmos.
598 Sci., doi:10.1175/JAS-D-15-0364.1, 2016.
599 Lappen, C. L. and Randall, D. A.: Toward a unified parameterization of the boundary layer and moist
600 convection. Part I: A new type of mass-flux model, J. Atmos. Sci., doi:10.1175/1520-
601 0469(2001)058<2021:TAUPOT>2.0.CO;2, 2001.
602 Logan, T., Xi, B. and Dong, X.: Aerosol properties and their influences on marine boundary layer cloud
603 condensation nuclei at the ARM mobile facility over the Azores, J. Geophys. Res.,
604 doi:10.1002/2013JD021288, 2014.
605 Logan, T., Dong, X. and Xi, B.: Aerosol properties and their impacts on surface CCN at the ARM
606 Southern Great Plains site during the 2011 Midlatitude Continental Convective Clouds
607 Experiment, Adv. Atmos. Sci., doi:10.1007/s00376-017-7033-2, 2018.
608 Lu, M. L., Conant, W. C., Jonsson, H. H., Varutbangkul, V., Flagan, R. C. and Seinfeld, J. H.: The marine
609 stratus/stratocumulus experiment (MASE): Aerosol-cloud relationships in marine stratocumulus, J.
610 Geophys. Res., doi:10.1029/2006JD007985, 2007.
611 Mann, J. A., Christine Chiu, J., Hogan, R. J., O'Connor, E. J., L'Ecuyer, T. S., Stein, T. H. and Jefferson,
612 A.: Aerosol impacts on drizzle properties in warm clouds from ARM Mobile Facility maritime and
613 continental deployments, J. Geophys. Res., doi:10.1002/2013JD021339, 2014.

614 Martin, G. M., Johnson, D. W. and Spice, A.: The Measurement and Parameterization of Effective Radius
615 of Droplets in Warm Stratocumulus Clouds, J. Atmos. Sci., doi:10.1175/1520-
616 0469(1994)051<1823:tmapoe>2.0.co;2, 1994.
617 Martins, J. V., Marshak, A., Remer, L. A., Rosenfeld, D., Kaufman, Y. J., Fernandez-Borda, R., Koren,
618 I., Correia, A. L., Zubko, V. and Artaxo, P.: Remote sensing the vertical profile of cloud droplet
619 effective radius, thermodynamic phase, and temperature, Atmos. Chem. Phys., doi:10.5194/acp-11-
620 9485-2011, 2011.
621 McComiskey, A, Feingold, G., Frisch, A. S., Turner, D. D., Miller, M., Chiu, J. C., Min, Q. and Ogren,
622 J.: An assessment of aerosol-cloud interactions in marine stratus clouds based on surface remote
623 sensing, J. Geophys. Res., 114, D09203, doi:10.1029/2008JD011006, 2009.
624 McComiskey, A. and Feingold, G.: The scale problem in quantifying aerosol indirect effects, Atmos.
625 Chem. Phys., doi:10.5194/acp-12-1031-2012, 2012.
626 Medeiros, B. and Stevens, B.: Revealing differences in GCM representations of low clouds, Clim. Dyn.,
627 doi:10.1007/s00382-009-0694-5, 2011.
628 Morris, V. R.: Ceilometer Instrument Handbook, DOE ARM Climate Research Facility, DOE/SC-
629 ARM-TR-020, 2016. Available at:
630 https://www.arm.gov/publications/tech_reports/handbooks/ceil_handbook.pdf, last access: 23
631 April 2021.
632 Newsom, R. K., Sivaraman, C., Shippert, T.R. and Riihimaki, L. D.: Doppler Lidar Vertical Velocity
633 Statistics Value-Added Product. DOE ARM Climate Research Facility, DOE/SC-ARM/TR-149,
634 2019. Available at: https://www.arm.gov/publications/tech_reports/doe-sc-arm-tr-149.pdf, last
635 access: 23 April 2021.
636 Nicholls, S.: The dynamics of stratocumulus: Aircraft observations and comparisons with a mixed layer
637 model, Q. J. R. Meteorol. Soc., doi:10.1002/qj.49711046603, 1984.
638 Pandithurai, G., Takamura, T., Yamaguchi, J., Miyagi, K., Takano, T., Ishizaka, Y., Dipu, S. and Shimizu,
639 A.: Aerosol effect on cloud droplet size as monitored from surface-based remote sensing over East
640 China Sea region, Geophys. Res. Lett., doi:10.1029/2009GL038451, 2009.

https://doi.org/10.5194/acp-2021-391
Preprint. Discussion started: 7 June 2021


Atmospheric Chemistry and Physics Discussions

641 Pawlowska, H., Grabowski, W. W. and Brenguier, J. L.: Observations of the width of cloud droplet
642 spectra in stratocumulus, Geophys. Res. Lett., doi:10.1029/2006GL026841, 2006.
643 Pearson, G., Davies, F. and Collier, C.: An analysis of the performance of the UFAM pulsed Doppler
644 lidar for observing the boundary layer, J. Atmos. Ocean. Technol.,
645 doi:10.1175/2008JTECHA1128.1, 2009.
646 Pinsky, M. B. and Khain, A. P.: Effects of in-cloud nucleation and turbulence on droplet spectrum
647 formation in cumulus clouds, Q. J. R. Meteorol. Soc., doi:10.1256/003590002321042072, 2002.
648 Rosenfeld, D. and Woodley, W. L.: Closing the 50-year circle: From cloud seeding to space and back to
649 climate change through precipitation physics. Chapter 6 of "Cloud Systems, Hurricanes, and the
650 Tropical Rainfall Measuring Mission (TRMM)", edited by: Tao, W.-K. and Adler, R. F., Meteor.
651 Monogr., 51, 234 pp., 59–80, AMS, 2003.
652 Rosenfeld, D.: Aerosol-Cloud Interactions Control of Earth Radiation and Latent Heat Release Budgets,
653 in Solar Variability and Planetary Climates., 2007.
654 Rosenfeld, D., Wang, H. and Rasch, P. J.: The roles of cloud drop effective radius and LWP in
655 determining rain properties in marine stratocumulus, Geophys. Res. Lett.,
656 doi:10.1029/2012GL052028, 2012.
657 Rosenfeld, D., Zhu, Y., Wang, M., Zheng, Y., Goren, T. and Yu, S.: Aerosol-driven droplet
658 concentrations dominate coverage and water of oceanic low-level clouds, Science (80-.).,
659 doi:10.1126/science.aav0566, 2019.
660 Seinfeld, J. H., Bretherton, C., Carslaw, K. S., Coe, H., DeMott, P. J., Dunlea, E. J., Feingold, G., Ghan,
661 S., Guenther, A. B., Kahn, R., Kraucunas, I., Kreidenweis, S. M., Molina, M. J., Nenes, A., Penner,
662 J. E., Prather, K. A., Ramanathan, V., Ramaswamy, V., Rasch, P. J., Ravishankara, A. R., Rosenfeld,
663 D., Stephens, G. and Wood, R.: Improving our fundamental understanding of the role of aerosol-
664 cloud interactions in the climate system, Proc. Natl. Acad. Sci. U. S. A.,
665 doi:10.1073/pnas.1514043113, 2016.

666 Siebert, H., Szodry, K.-E., Egerer, U., Wehner, B., Henning, S., Chevalier, K., Lückerath, J., Welz, O.,
667 Weinhold, K., Lauermann, F., Gottschalk, M., Ehrlich, A., Wendisch, M., Fialho, P., Roberts, G.,
668 Allwayin, N., Schum, S., Shaw, R. A., Mazzoleni, C., Mazzoleni, L., Nowak, J. L., Malinowski, S.
669 P., Karpinska, K., Kumala, W., Czyzewska, D., Luke, E. P., Kollias, P., Wood, R. and Mellado, J.
670 P.: Observations of Aerosol, Cloud, Turbulence, and Radiation Properties at the Top of the Marine
671 Boundary Layer over the Eastern North Atlantic Ocean: The ACORES Campaign, Bull. Am.
672 Meteorol. Soc., doi:10.1175/bams-d-19-0191.1, 2021.
673 Thorsen, T. J. and Fu, Q.: Automated retrieval of cloud and aerosol properties from the ARM Raman
674 Lidar. Part II: Extinction, J. Atmos. Ocean. Technol., doi:10.1175/JTECH-D-14-00178.1, 2015.
675 Twohy, C. H., Petters, M. D., Snider, J. R., Stevens, B., Tahnk, W., Wetzel, M., Russell, L. and Burnet,
676 F.: Evaluation of the aerosol indirect effect in marine stratocumulus clouds: Droplet number, size,
677 liquid water path, and radiative impact, J. Geophys. Res. D Atmos., doi:10.1029/2004JD005116,
678 2005.
679 Twomey, S.: The nuclei of natural cloud formation part II: The supersaturation in natural clouds and the
680 variation of cloud droplet concentration, Geofis. Pura e Appl., doi:10.1007/BF01993560, 1959.
681 Twomey, S.: The Influence of Pollution on the Shortwave Albedo of Clouds, J. Atmos. Sci.,
682 doi:10.1175/1520-0469(1977)034<1149:TIOPOT>2.0.CO;2, 1977.
683 Wang, Y., Zheng, X., Dong, X., Xi, B., Wu, P., Logan, T., and Yung, Y. L.: Impacts of long-range
684 transport of aerosols on marine-boundary-layer clouds in the eastern North Atlantic, Atmos. Chem.
685 Phys., 20, 14741–14755, https://doi.org/10.5194/acp-20-14741-2020, 2020.
686 West, R. E. L., Stier, P., Jones, A., Johnson, C. E., Mann, G. W., Bellouin, N., Partridge, D. G. and
687 Kipling, Z.: The importance of vertical velocity variability for estimates of the indirect aerosol
688 effects, Atmos. Chem. Phys., doi:10.5194/acp-14-6369-2014, 2014.
689 Widener, K, Bharadwaj, N, and Johnson, K: Ka-Band ARM Zenith Radar (KAZR) Instrument Handbook.
690 DOE ARM Climate Research Facility, DOE/SC-ARM/TR-106, 2012. Available at:

https://www.arm.gov/publications/tech_reports/handbooks/kazr_handbook.pdf, last access: 23 April 2021.

Wood, R.: Rate of loss of cloud droplets by coalescence in warm clouds, J. Geophys. Res. Atmos., doi:10.1029/2006JD007553, 2006.

Wood, R. and Bretherton, C. S.: On the relationship between stratiform low cloud cover and lower-tropospheric stability, J. Clim., doi:10.1175/JCLI3988.1, 2006.

Wood, R.: Stratocumulus clouds, Mon. Weather Rev., doi:10.1175/MWR-D-11-00121.1, 2012.

Wood, R., Wyant, M., Bretherton, C. S., Rémillard, J., Kollias, P., Fletcher, J., Stemmler, J., De Szoeke, S., Yuter, S., Miller, M., Mechem, D., Tselioudis, G., Chiu, J. C., Mann, J. A. L., O'Connor, E. J., Hogan, R. J., Dong, X., Miller, M., Ghate, V., Jefferson, A., Min, Q., Minnis, P., Palikonda, R., Albrecht, B., Luke, E., Hannay, C. and Lin, Y.: Clouds, aerosols, and precipitation in the marine boundary layer: An arm mobile facility deployment, Bull. Am. Meteorol. Soc., doi:10.1175/BAMS-D-13-00180.1, 2015.

Wu, P., Dong, X. and Xi, B.: Marine boundary layer drizzle properties and their impact on cloud property retrieval, Atmos. Meas. Tech., doi:10.5194/amt-8-3555-2015, 2015.

Wu, P., Dong, X., Xi, B., Tian, J. and Ward, D. M.: Profiles of MBL Cloud and Drizzle Microphysical Properties Retrieved From Ground-Based Observations and Validated by Aircraft In Situ Measurements Over the Azores, J. Geophys. Res. Atmos., doi:10.1029/2019JD032205, 2020a.

Wu, P., Dong, X. and Xi, B.: A climatology of marine boundary layer cloud and drizzle properties derived from ground-based observations over the azores, J. Clim., doi:10.1175/JCLI-D-20-0272.1, 2020b.

Xi, B., Dong, X., Minnis, P. and Khaiyer, M. M.: A 10 year climatology of cloud fraction and vertical distribution derived from both surface and GOES observations over the DOE ARM SPG site, J. Geophys. Res. Atmos., doi:10.1029/2009JD012800, 2010.

715 Yue, Q., Kahn, B. H., Fetzer, E. J. and Teixeira, J.: Relationship between marine boundary layer clouds
716 and lower tropospheric stability observed by AIRS, CloudSat, and CALIOP, J. Geophys. Res.
717 Atmos., doi:10.1029/2011JD016136, 2011.
718 Yum, S. S., Wang, J., Liu, Y., Senum, G., Springston, S., McGraw, R. and Yeom, J. M.: Cloud
719 microphysical relationships and their implication on entrainment and mixing mechanism for the
720 stratocumulus clouds measured during the VOCALS project, J. Geophys. Res.,
721 doi:10.1002/2014JD022802, 2015.
722 Zhang, S., Wang, M., J. Ghan, S., Ding, A., Wang, H., Zhang, K., Neubauer, D., Lohmann, U., Ferrachat,
723 S., Takeamura, T., Gettelman, A., Morrison, H., Lee, Y., T. Shindell, D., G. Partridge, D., Stier, P.,
724 Kipling, Z. and Fu, C.: On the characteristics of aerosol indirect effect based on dynamic regimes
725 in global climate models, Atmos. Chem. Phys., doi:10.5194/acp-16-2765-2016, 2016.
726 Zawadowicz, M. A., Suski, K., Liu, J., Pekour, M., Fast, J., Mei, F., Sedlacek, A., Springston, S., Wang,
727 Y., Zaveri, R. A., Wood, R., Wang, J., and Shilling, J. E.: Aircraft measurements of aerosol and
728 trace gas chemistry in the Eastern North Atlantic, Atmos. Chem. Phys. Discuss. [preprint],
729 https://doi.org/10.5194/acp-2020-887, in review, 2020.
730 Zheng, G., Wang, Y., Aiken, A. C., Gallo, F., Jensen, M. P., Kollias, P., Kuang, C., Luke, E., Springston,
731 S., Uin, J., Wood, R., and Wang, J.: Marine boundary layer aerosol in the eastern North Atlantic:
732 seasonal variations and key controlling processes, Atmos. Chem. Phys., 18, 17615–17635,
733 https://doi.org/10.5194/acp-18-17615-2018, 2018.
734 Zheng, G., Kuang, C., Uin, J., Watson, T., and Wang, J.: Large contribution of organics to condensational
735 growth and formation of cloud condensation nuclei (CCN) in the remote marine boundary layer,
736 Atmos. Chem. Phys., 20, 12515–12525, https://doi.org/10.5194/acp-20-12515-2020, 2020.
737 Zheng, X., Xi, B., Dong, X., Logan, T., Wang, Y. and Wu, P.: Investigation of aerosol-cloud interactions
738 under different absorptive aerosol regimes using Atmospheric Radiation Measurement (ARM)

https://doi.org/10.5194/acp-2021-391
Preprint. Discussion started: 7 June 2021

Atmospheric Chemistry and Physics Discussions

739 southern Great Plains (SGP) ground-based measurements, Atmos. Chem. Phys., doi:10.5194/acp-
740 20-3483-2020, 2020.
741 Zhu, P. and Zuidema, P.: On the use of PDF schemes to parameterize sub-grid clouds, Geophys. Res.
742 Lett., doi:10.1029/2008GL036817, 2009.
743
744
745
746
747
748
749
750
751
752
753
754
755
756
757
758
759
760
761
762

https://doi.org/10.5194/acp-2021-391
Preprint. Discussion started: 7 June 2021

Atmospheric Chemistry and Physics Discussions

Table 1. Dates and time periods of selected non-precipitating MBL cloud periods

Case No.	Start Date	Start UTC	End Date	End UTC	Valid Samples
1	20160915	2200	20160916	0020	24
2	20170219	2110	20170220	0520	87
3	20170222	0830	20170222	1200	38
4	20170605	1430	20170605	1900	54
5	20170616	1230	20170616	1510	32
6	20170617	0320	20170617	0520	24
7	20170627	0020	20170627	0250	28
8	20170630	0530	20170630	0930	42
9	20170630	1400	20170630	1700	34
10	20170706	0140	20170706	0900	62
11	20170707	0130	20170707	1000	91
12	20170910	2100	20170911	0600	94
13	20170911	1930	20170911	2150	24
14	20170912	0820	20170912	1100	32
15	20171006	2110	20171006	2320	26
16	20180130	1030	20180131	0500	152
17	20180203	1930	20180204	0500	72
18	20180324	0210	20180324	0600	46
19	20180508	0730	20180508	1110	42
20	20180513	2130	20180514	1200	139

https://doi.org/10.5194/acp-2021-391
Preprint. Discussion started: 7 June 2021

Atmospheric Chemistry and Physics Discussions

Table 2. Occurrence frequencies of large in-cloud r_e* under high PWV conditions

PWV (cm)	2.2-2.4	2.4-2.6	2.6-2.8	2.8-3.0	3.0-3.2	3.2-3.4
r_e > 12 μm (%)	22.4	32.0	51.2	70.1	96.5	95.1
r_e > 14 μm (%)	1.72	2.41	4.35	16.4	35.1	9.76

*The occurrence of large r_e is defined when the r_e is found to be larger than 12 μm or 14 μm using the retrieved in-cloud vertical profiles.

https://doi.org/10.5194/acp-2021-391
Preprint. Discussion started: 7 June 2021

Atmospheric Chemistry and Physics Discussions

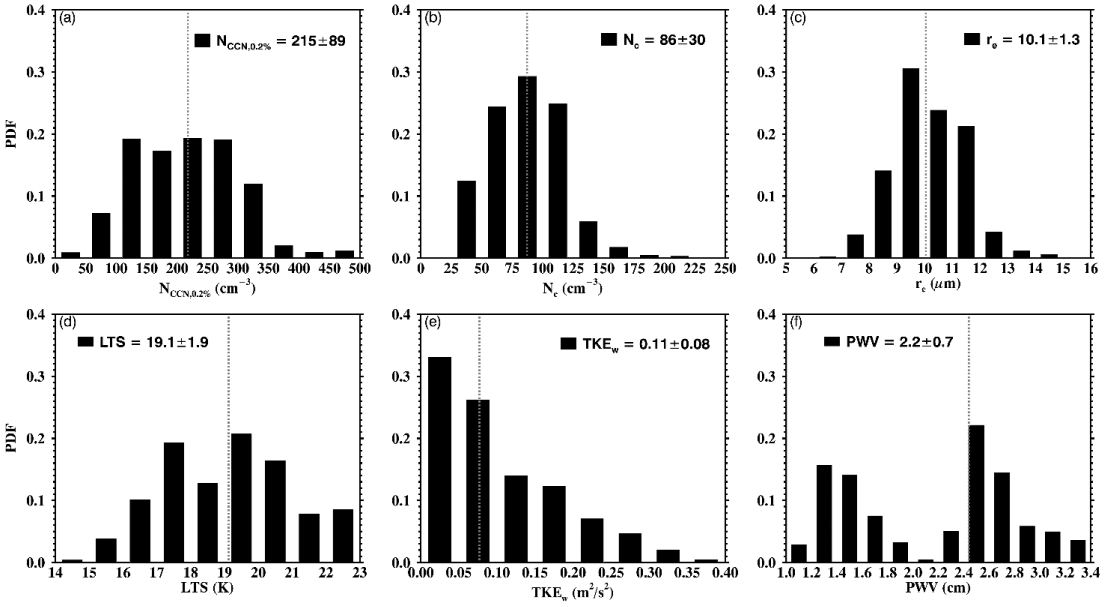

Figure 1. Probability distribution functions (PDFs), mean, standard deviation and median values (dash lines) of aerosol, cloud and meteorological properties for 20 selected non-precipitating cloud cases at the DOE ENA site during the period 2016-2018. (a) Cloud condensation nuclei (CCN) number concentration at 0.2% supersaturation ($N_{CCN,0.2\%}$), (b) cloud-droplet number concentration (N_c), (c) cloud-droplet effective radius (r_e), (d) lower tropospheric stability (LTS), (e) mean vertical component of turbulence kinetic energy ($\mathrm{TKE_w}$), and (f) precipitable water vapor (PWV).

https://doi.org/10.5194/acp-2021-391
Preprint. Discussion started: 7 June 2021

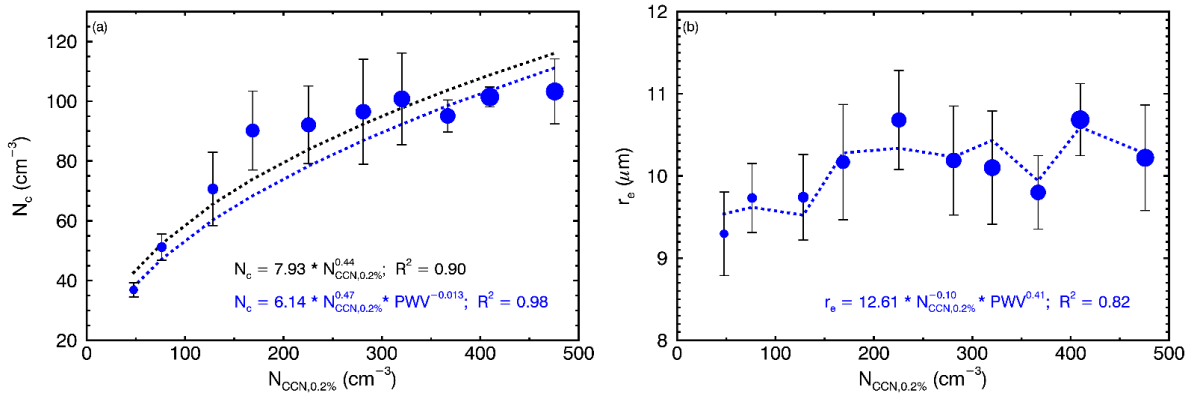

Figure 2. (a) N_c and (b) r_e as a function of $N_{CCN,0.2\%}$ (x-axis) and PWV (blue filled circles) for all selected samples. The larger blue circles represent relatively higher PWV values. Whiskers denote one standard deviation for each bin.

https://doi.org/10.5194/acp-2021-391
Preprint. Discussion started: 7 June 2021

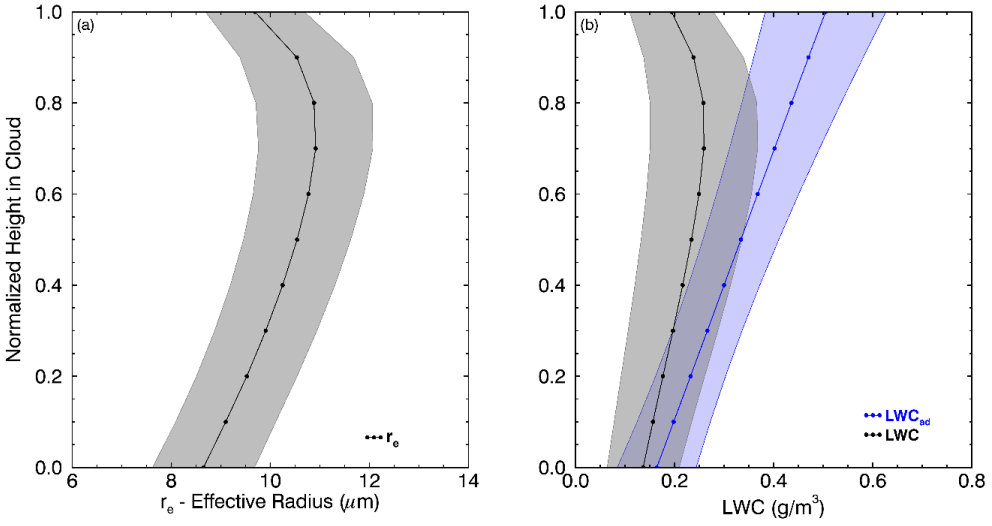

Figure 3. Normalized in-cloud vertical profiles of retrieved (a) r_e and (b) LWC (black) and calculated adiabatic LWC_{ad} (blue) for all selected cloud cases, 0 is cloud base and 1 is cloud top. Solid dotted lines denote mean values and shaded area denote one standard deviation at each height.

https://doi.org/10.5194/acp-2021-391
Preprint. Discussion started: 7 June 2021

Atmospheric Chemistry and Physics Discussions

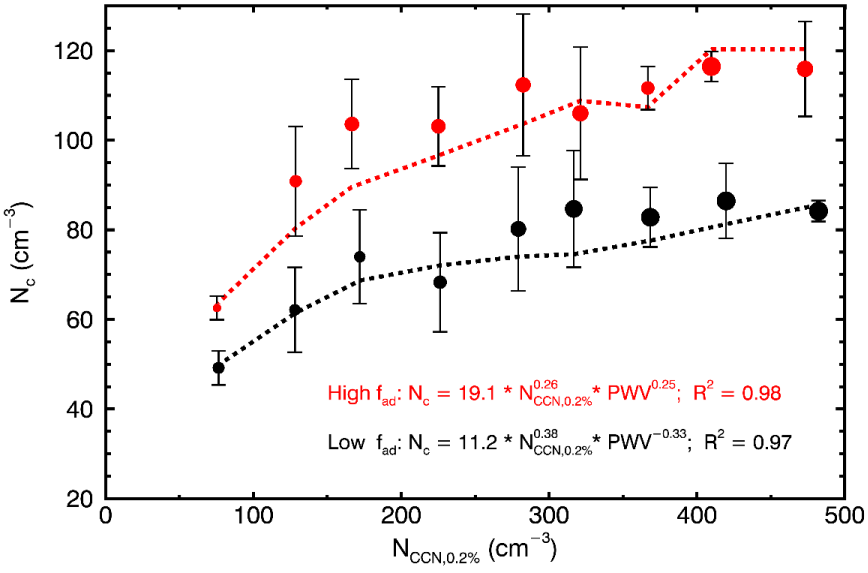

Figure 4. N_c as a function of $N_{CCN,0.2\%}$ (x-axis) and PWV (dots) for high adiabaticity f_{ad} (red) and low f_{ad} (black) regimes. The larger circles represent relatively higher PWV values. Whiskers denote one standard deviation for each bin.

https://doi.org/10.5194/acp-2021-391
Preprint. Discussion started: 7 June 2021

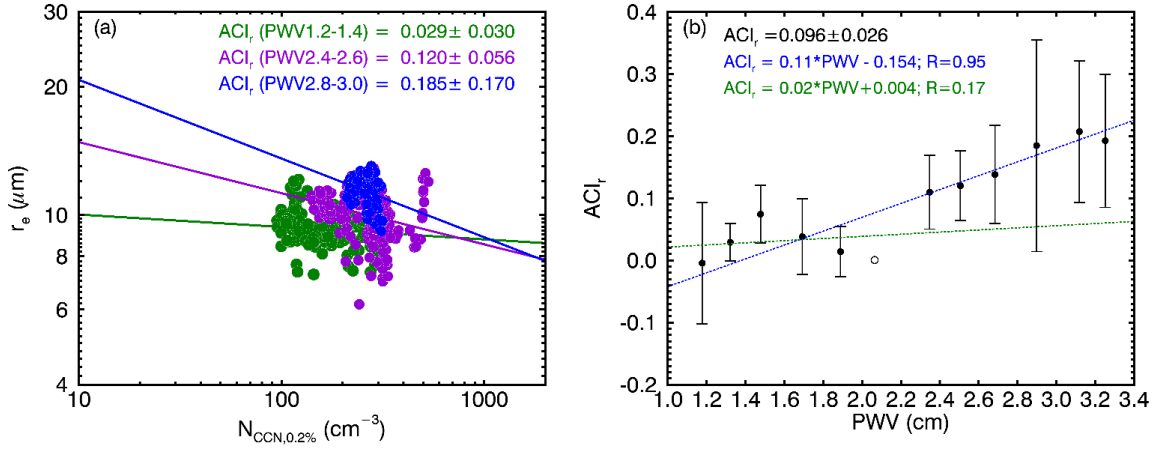

Figure 5. ACI_r derived from (a) r_e to $N_{CCN,0.2\%}$ in following three PWV bins: 1.2-1.4 cm (green), 2.4-2.6 cm (purple), 2.8-3.0 cm (blue) and (b) Relationship of ACI_r (dots) to binned PWV. Whiskers denote one standard deviation for each bin. Linear regressions are performed in relatively low PWV regime (< 2.0 cm, green) and high PWV regime (> 2.2 cm). Bin that does not pass the significant test in 95% confidence level is denoted by a hollow circle and is excluded from the regressions. ACI_r represents the relative change of r_e with respect to the relative change of $N_{CCN,0.2\%}$, where positive ACI_r denotes the decrease of r_e with increased $N_{CCN,0.2\%}$ under binned PWV.

https://doi.org/10.5194/acp-2021-391
Preprint. Discussion started: 7 June 2021

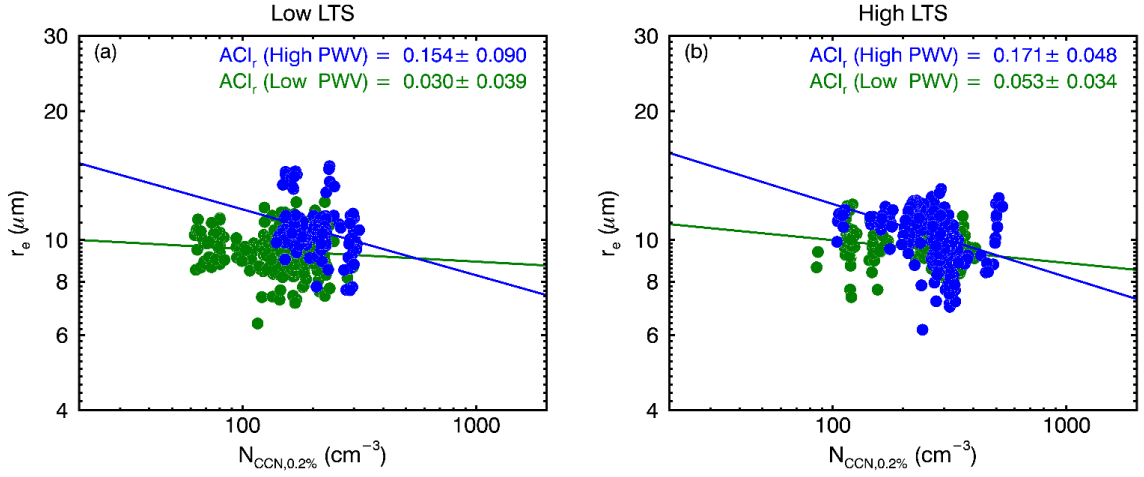

Figure 6. ACI$_r$ derived from r_e to $N_{CCN,0.2\%}$ for (a) low LTS and (b) high LTS regimes. Samples in the low PWV regime are plotted in green, and samples in the high PWV regime are plotted in blue.

https://doi.org/10.5194/acp-2021-391
Preprint. Discussion started: 7 June 2021

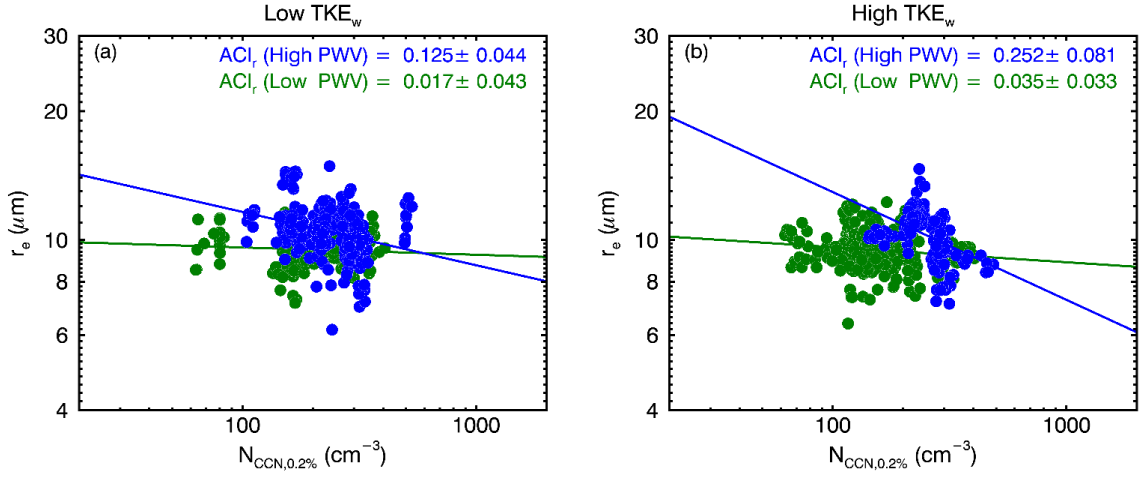

Figure 7. ACI_r derived from r_e to $N_{CCN,0.2\%}$ for (a) low TKE_w and (b) high TKE_w regimes. Samples in the low PWV regime are plotted in green, and samples in the high PWV regime are plotted in blue.